2003ESASP.535..541

3-D SIMULATIONS OF ICMES BY COUPLED CORONAL AND HELIOSPHERIC MODELS

D. Odstrcil *[1], P. Riley[2], J. A. Linker[2], R. Lionello[2], Z. Mikic[2], and V. J. Pizzo[3]

[1]University of Colorado, CIRES-NOAA/SEC, 325 Broadway, Boulder, CO 80305, USA
[2]Science Applications International Corporation, San Diego, CA 92121, USA
[3]NOAA/Space Environment Center, 325 Broadway, Boulder, CO 80305, USA

ABSTRACT

We overview the main features and approximations of the heliospheric modeling system based on a 3-D ideal magnetohydrodynamic (MHD) model that can be driven by various analytic, empirical, and numerical models of the solar corona. Results are presented for two different self-consistent simulations of Sun-to-Earth transient events: (1) propagation of an interplanetary magnetic flux rope driven by the 3-D MHD coronal model; and (2) the May 12-15, 1997 interplanetary event driven by an empirical model of the ambient solar wind and fitted parameters for the halo coronal mass ejection (CME).

Key words: coronal mass ejection, magnetic flux rope, solar wind, interplanetary shock, magnetohydrodynamic model, numerical simulation.

1. INTRODUCTION

Coronal mass ejections (CMEs) and their interplanetary counterparts (ICMEs) represent different aspects of the same solar-terrestrial phenomena responsible for large geomagnetic storms. Because of the great complexity and huge spatial distance between the Sun and Earth these individual aspects have typically been investigated separately. This approach is useful for revealing the basic underlying physics; however, a complete picture requires a comprehensive model of all of the processes considered together.

Numerical magnetohydrodynamic (MHD) models are capable of predicting solar wind parameters at Earth, provided that appropriate time-dependent conditions are specified near the Sun. Since the knowledge of such conditions is at present insufficient to directly drive the numerical models, various approximations are used.

In this paper, we overview the main features and approximations of the heliospheric modeling system based on a 3-D ideal MHD model that can be driven by various analytic, empirical, and numerical models of the solar corona. We illustrate its abilities and limitations by simulating: (1) the propagation of an interplanetary magnetic flux rope and (2) the May 12-15, 1997 interplanetary event.

2. BACKGROUND

We are interested in modeling solar wind phenomena that result in conditions determining geomagnetic storms. Thus, we need to simulate parameters of the magnetic field, flow velocity, mass density, and temperature, for both ambient solar wind and transient disturbances. Figure 1 illustrates the large variations in plasma parameters between the Sun and Earth. Different regions involve different physical phenomena and processes that lead to the development of different models. On a large scale, it is convenient to distinguish between the "coronal" and "heliospheric" regions with an interface located in the super-critical flow region, usually between 18 and 30 R_S (see Fig. 2). While various plasma heating processes cause acceleration of the solar wind in the corona, it expands mostly adiabatically in the heliosphere. Further, while the background magnetic field plays an important role in the corona, it is passively convected in the heliosphere. Coronal models thus need to simulate more complex physical processes while heliospheric models can use simpler approximations over a much larger spatial domain. Computationally, it is also more efficient to advance the heliospheric portion of the simulation independently of the coronal time step. Note that the location of the model interface in a super-critical region significantly simplifies the numerical treatment of boundary conditions because information is passed only one way: from the coronal model to the heliospheric model.

*on leave from the Astronomical Institute, Academy of Sciences of the Czech Republic, 25165 Ondřejov, Czech Republic

Proc. ISCS 2003 Symposium, 'Solar Variability as an Input to the Earth's Environment', Tatranská Lomnica, Slovakia, 23-28 June 2003 (ESA SP-535, September 2003)

© European Space Agency • Provided by the NASA Astrophysics Data System

2003ESASP.535..5410

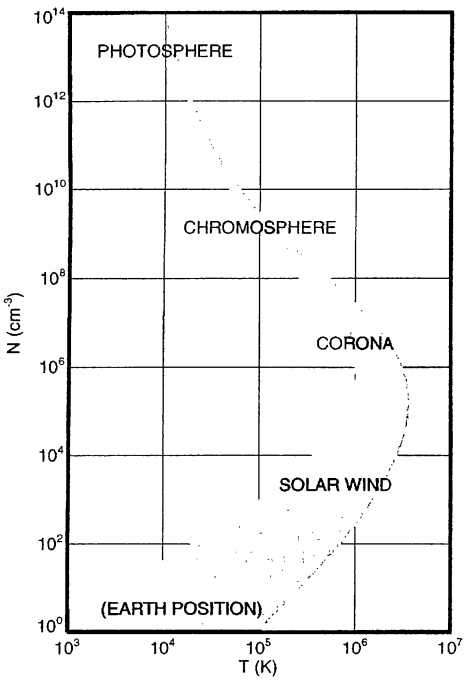

Figure 1. Diagram of plasma temperature and number density for different regions of space plasma (adapted from D. L. Book, NRL Plasma Formulary, NRL Publ. 0084-4040, Washington DC, 1987).

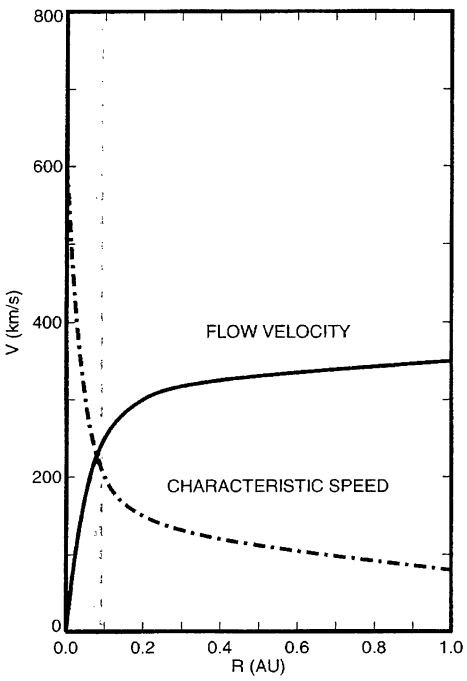

Figure 2. Typical values of the solar wind flow velocity (solid line) and a characteristic speed (the sum of the sound and Alfven speeds, dash-dotted line) as function of heliocentric distance. Vertical bars show the boundary between sub- and super-critical flow regions.

3. NUMERICAL MODELING SYSTEM

Our numerical modeling system is based on a 3-D MHD heliospheric model that can be driven by various analytic, empirical, and numerical models of the solar corona.

3.1. 3-D MHD Heliospheric Model

The heliospheric code Enlil is based on the 3-D ideal MHD description with two additional continuity equations used for tracing the injected CME material and the magnetic field polarity (see *Odstrcil and Pizzo* (1999) for details). The ratio of specific heats, γ, is 1.5. A modified high-resolution explicit finite-difference total-variation-diminishing (TVD) Lax-Friedrichs scheme is used (*Toth and Odstrcil,* 1996).

3.2. 3-D MHD Coronal Model

The coronal model is based on the 3-D resistive MHD equations that are solved by a semi-implicit finite-difference scheme using staggered meshes (*Mikic and Linker,* 1994; *Linker and Mikic,* 1995). The coronal model uses a ratio of specific heats $\gamma = 1.05$ to crudely simulate heat conduction processes and thermal energy sources.

3.3. Ambient Solar Wind

The SAIC group have established a repository of synoptic maps of the magnetic field and flow velocity at 30 R_S (*Linker et al.,* 1999; *Riley et al.,* 2001), http://sun.saic.com/mhdweb). The flow velocity is derived via empirical relations using the boundary between open and closed magnetic field lines obtained from the 3-D MHD coronal solution (see *Riley et al.* (2001) for details). The coronal solution itself is determined using the photospheric magnetic field observations from the National Solar Observatory at Kitt Peak (http://nsokp.nso.edu, http://synoptic.nso.edu).

3.4. Transient Disturbances

The cone model has been applied to reproduce the expanding halo CME observed by the LASCO/C3 coronagraph on May 12, 1997 (*Zhao et al.,* 2002). The best fit suggested an angular width of 50° and a central axis of the cone pointing to N3.0 and W1.0.

© European Space Agency • Provided by the NASA Astrophysics Data System

2003ESASP.535..5410

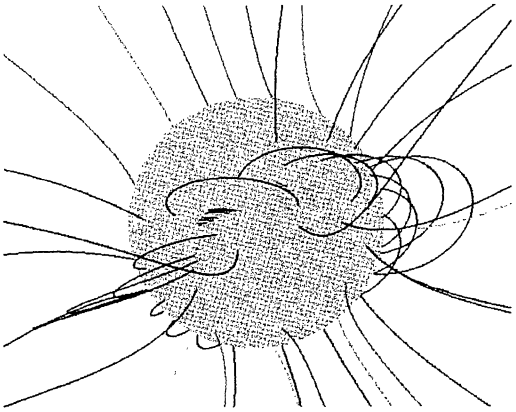

Figure 3. Global view of a magnetic flux rope formed in the solar corona within a sheared magnetic arcade. The computations were performed using the SAIC 3-D MHD coronal model.

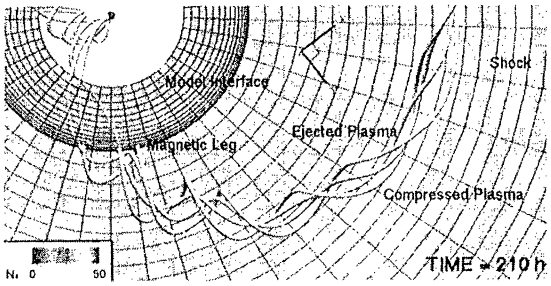

Figure 4. Global view of the interplanetary disturbance generated by an expanding flux rope initiated at the Sun, viewed from above the equatorial plane. The plasma number density (normalized to 1 AU) is shown in the equatorial plane. The solid lines show the numerical mesh at each 8th grid point.

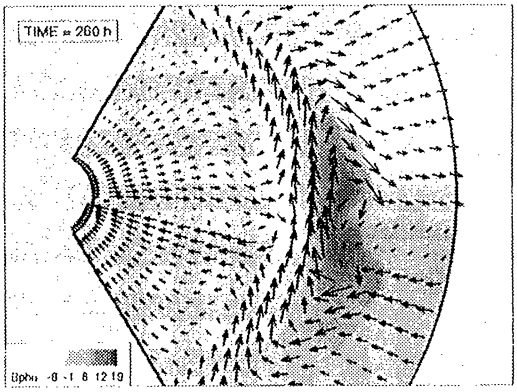

Figure 5. Global view of the interplanetary disturbance generated by a solar magnetic eruption. The magnetic field vectors and intensity of the azimuthal magnetic field component are shown in the meridional plane.

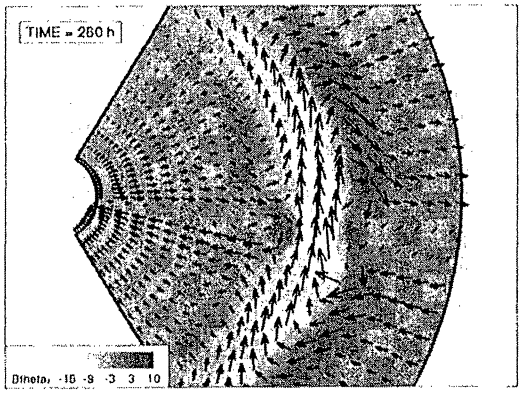

Figure 6. Global view of the interplanetary disturbance generated by a solar magnetic eruption. The magnetic field vectors and intensity of the meridional magnetic field component are shown in the meridional plane.

The CME was determined to be traveling at 650 km/s at 24 R_S (observed at 14:15:05 UT) and was accelerating with about 18.5 m s^{-2}. We have estimated that the leading edge of the CME reached a height of 30 R_S at 15:30 UT with a speed of 700 km/s, and it took approximately 8 hours for the CME to pass through that position (*Odstrcil et al.,* 2003). Further, we approximate the CME using a hydrodynamic plasma cloud that has about eight times larger pressure than the surrounding medium at 30 R_S.

4. RESULTS AND DISCUSSION

Here we present two examples of our results from the ongoing work within the NSF/CISM (http://www.bu.edu/cism) and DoD-AFOSR/MURI (http://solarmuri.ssl.berkeley.edu) projects.

4.1. Propagation of Interplanetary Flux Rope

Recently, we have successfully merged our 2.5-D MHD coronal and heliospheric models (*Odstrcil et al.,* 2002a). Here we present some new heliospheric results from the ongoing coupled 3-D MHD simulations (see also (*Odstrcil et al.,* 2002b)) for a hypothetical case involving a magnetic flux rope, shock, streamer belt, and current sheet.

Magnetic flux cancellation in a helmet streamer configuration energized by a shear flow first leads to the formation of a stable flux rope structure. When a critical threshold of flux reduction is exceeded, the configuration erupts violently (see *Linker et al.,* (2003) for details). Figure 3 shows an early phase of the eruption of a magnetic flux rope (simulated by the 3-D MHD coronal model). A significant amount

© European Space Agency • Provided by the NASA Astrophysics Data System

2003ESASP.535..5410

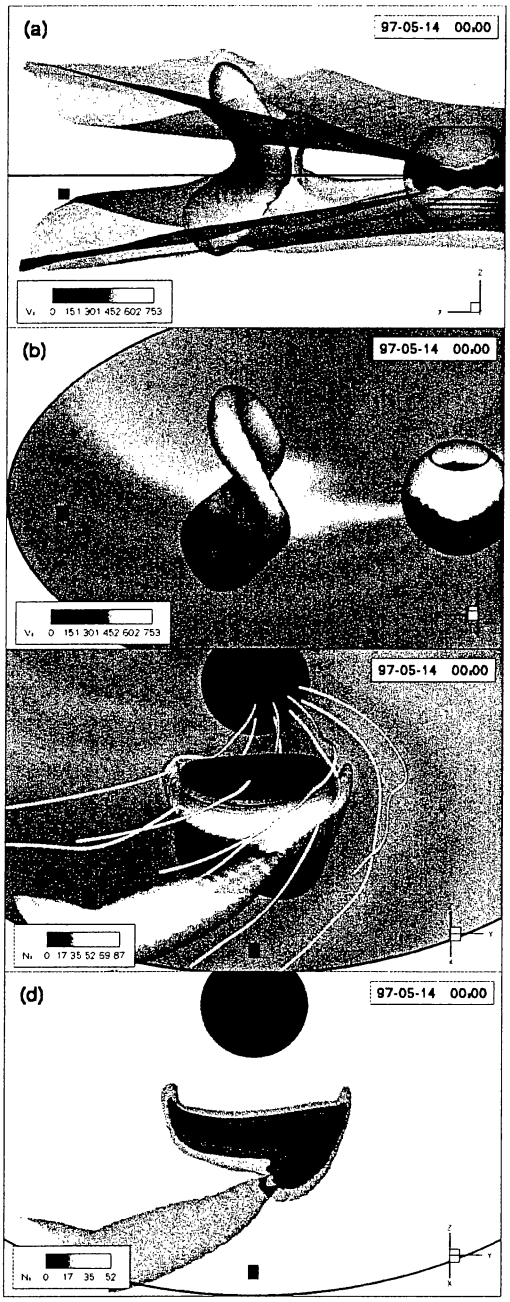

Figure 7. Visualization of solar wind parameters on May 14 00:00 UT. The injected cloud is shown as an iso-surface at 25% of the maximum value of its density (scaled by $1/r^2$) in panels a-c. The flow velocity is shown on the source surface in panels a-b, as boundaries between the slow and fast stream flows (panel a) and as a distribution on the equatorial plane (panel b). The number density is shown on the source surface (panels c-d) and as translucent iso-surfaces at 20 cm^{-3} (panel c) and 20, 30, and 50 cm^{-3} (panel d) of the scaled density. The magnetic field lines are shown as white lines in panel c. The equatorial plane is shown by a solid line and the Earth position is shown by a dark box in all panels.

of stored magnetic energy is released through magnetic reconnection and the ejected flux rope structure propagates out into the heliosphere. Figure 4 shows the expanding magnetic flux tope in interplanetary space (simulated by the 3-D MHD heliospheric model). The flux rope stretches from the Sun through the model interface boundary into the heliosphere and generates an interplanetary shock that compresses the plasma density ahead of the flux rope.

Figure 5 shows a detailed view at a later time. A portion of the shock wave interacts with the slow and dense streamer belt flow and a "dimple" is formed in the shock front (*Odstrcil et al.*, 1996). This causes the shock front to become oblique with respect to the north-south direction and meridional magnetic fields can be generated via shock compression of the ambient interplanetary magnetic field (which, originally, had negligible meridional component). Figure 6 shows the distribution of the meridional component of the magnetic field. It can be seen that behind the shock front the meridional component becomes positive in both northern and southern hemispheres, while later it becomes negative. This scenario is valid for a magnetic field configuration with positive and negative polarity in the northern and southern hemispheres, respectively. When the overall polarity is reversed, the meridional magnetic field will become first negative and then positive.

4.2. May 12-15, 1997 Interplanetary Event

We have chosen the well-defined halo-CME event of May 12, 1997 as our initial example because it is characterized by a relatively quiet solar and interplanetary background into which the ejecta was launched (*Webb et al.*, 2000).

Figures 7a-d show various visualizations of the traveling interplanetary disturbance. There are three large-scale effects as a result of dynamic interaction between the ICME and ambient solar wind. First, the injected ICME has much larger angular size than the streamer belt; thus different parts of the ICME propagate in the background solar wind with different convective velocities. This causes significant latitudinal distortion in the ICME shape, as can be seen in Figs. 7a and 7b. Second, the simulated ICME propagates slightly ahead of the moderate fast stream (Fig. 7b), and it propagates into the dense slow streamer belt (Fig. 7c). The fast stream results from an excursion of the southern coronal hole toward the equatorial plane. Faster flow from behind and dense slow plasma ahead favors significant compression of the ejecta. This is in agreement with observations (*Webb et al.*, 2000). Third, note that while the plasma cloud extends to high latitudes (Figs. 7a-c), the largest enhancement of the density is within the streamer belt (Fig. 7d). The ICME is launched with an initial speed about the same as that of the fast flow but approximately twice the speed of the heliospheric streamer belt flow. This causes significant compression of the injected plasma as well as

© European Space Agency • Provided by the NASA Astrophysics Data System

2003ESASP.535..5410

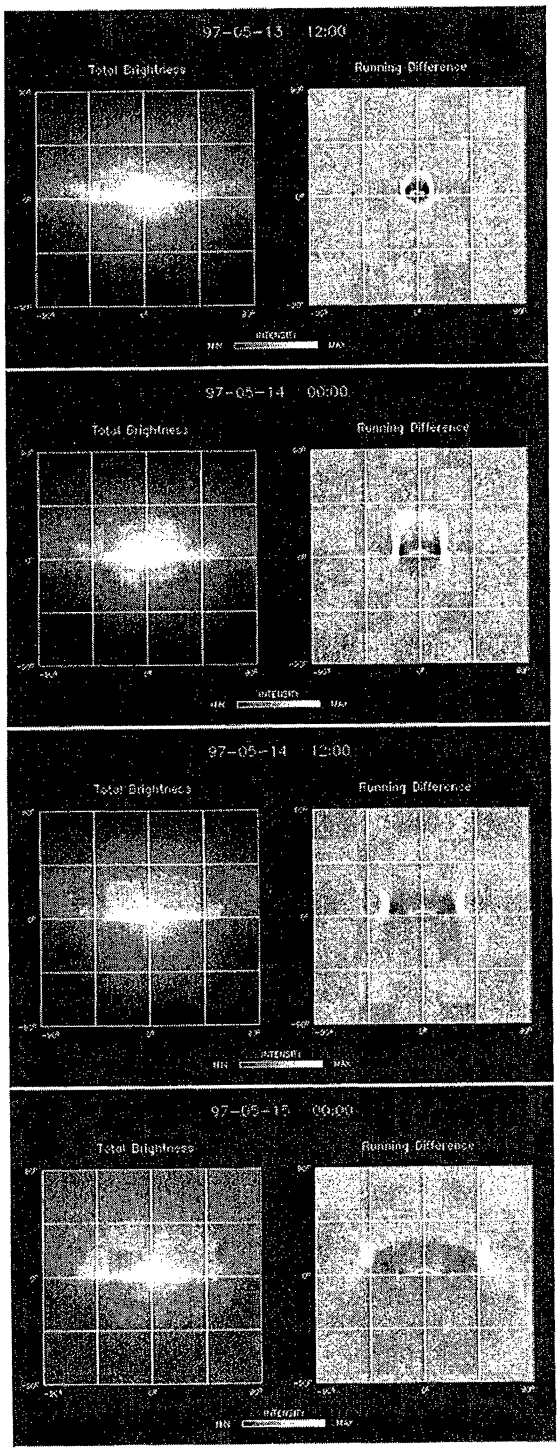

Figure 8. Synthetic white-light images as seen from Earth at different times. Panels on the left and right show total brightness and running difference of total brightness (difference of two images over 6-hour interval), respectively.

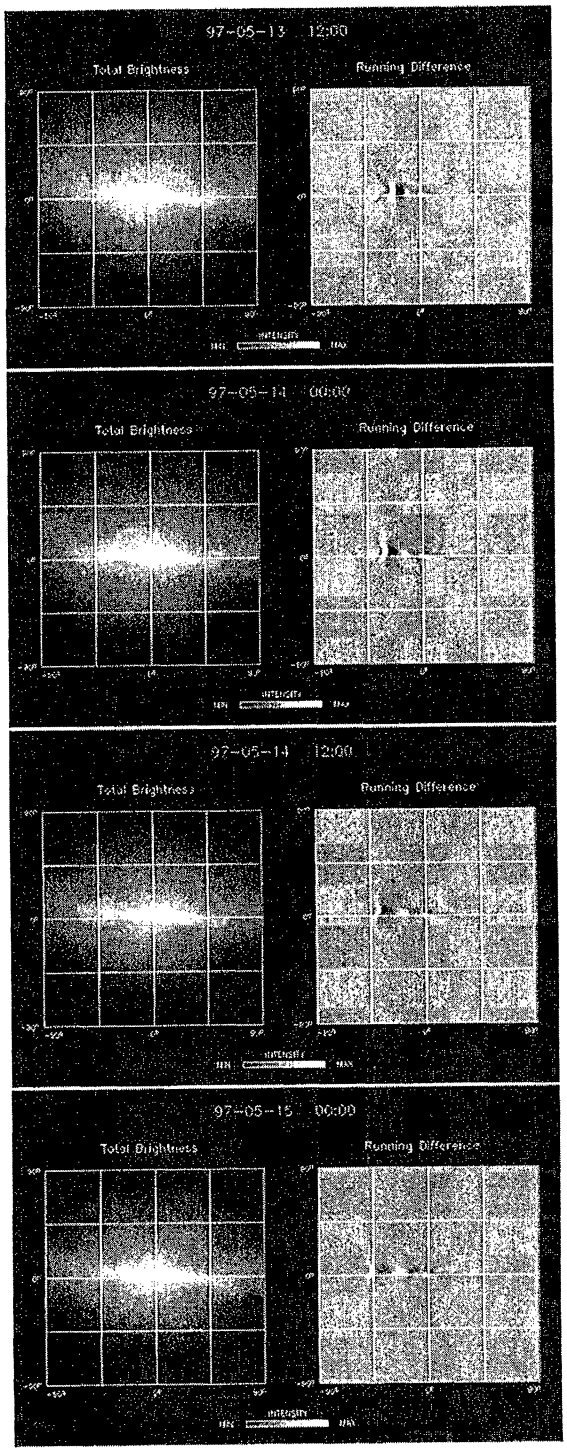

Figure 9. Same as in Fig. 8 but as seen from a 1 AU position in ecliptic plane located 90° westward from the Sun-Earth line.

© European Space Agency • Provided by the NASA Astrophysics Data System

2003ESASP.535..5410

the formation of a shock in this region, which can be seen as an arc-like high-density structure (Fig. 7d).

Figures 8 and 9 show synthetic white-light images generated from the 3-D density distribution as they might be observed from two vantage points at 1 AU. In addition to the total brightness, the running difference is shown as the difference from an image generated six hours earlier. Note that it is possible to identify the main morphology of the ICME although the initial enhancement of the simulated ICME was very moderate. The front view (Fig. 8) shows the ICME as a ring of enhanced brightness encircling the Sun. White-light intensity reflects the structure of the ICME that becomes strongly affected by its interaction with the bi-modal solar wind. Large density compression within the streamer belt results in brighter structures in the synthetic images. The side view (Fig. 9) shows the latitudinally distorted shape of the ICME. Enhanced brightness corresponds to the dense region within the streamer belt between the shock front and the plasma cloud as seen in Fig. 7c.

5. CONCLUSIONS

We have presented two examples of our current capabilities in numerical simulations of ICMEs by the 3-D MHD heliospheric code Enlil. This code can be driven by various analytic, empirical, and numerical models in order to investigate the dynamics of transient disturbances in interplanetary space, to study heliospheric consequences of various coronal models, and attempt to reproduce the basic features of observed events.

The results presented here illustrate two different self-consistent numerical simulations of Sun-to-Earth transient events. In coupled coronal and heliospheric 3-D MHD simulations, the interplanetary magnetic cloud is generated by a magnetic eruption in the solar corona. Thus, the simulated ICME is self-consistent with the surrounding solar wind parameters *ab initio*, and it allows us to follow the consequences of the solar activity directly and more realistically. However, while this approach is invaluable for increasing our understanding of transient phenomena, application to observed events is still under development. On the other hand, empirical models of the ambient solar wind and fitting of observed halo-CME events enables reproduction of some general features of the observed event and provide us with a global picture. However, the internal structure of the ICME (especially intensity and orientation of the magnetic field) is only crudely treated.

Major advances in supercomputing are now enabling high-resolution, three-dimensional simulations of global dynamical processes. We believe that computational resources are no longer the main obstacle to realistic simulations of interplanetary disturbances. The main challenges are in development of: (1) new and more sophisticated models of particular phenomena and (2) an over-arching framework. This framework should: (1) join individual models consistently using a "plug-and-play" approach and (2) permit straightforward incorporation of observational inputs and analysis tools. Of course, full understanding of heliospheric events will require new observational capabilities, especially multi-point observations at different heliocentric distances and longitudes. In summary, more effort is needed, and the resources of the entire space weather community will need to be tapped to assure success.

ACKNOWLEDGMENTS

This work has been supported by the DoD-AFOSR/MURI (Multi-Disciplinary Research Initiative) and NSF/CISM (Center for Integrated Space Weather Modeling) projects. Additional support was from NASA SEC and LWS programs, NSF SHINE program, and by grants A3003003 and S10030067 from the Academy of Sciences and Grant Agency of the Czech Republic. Computational facilities were provided by National Center for Atmospheric Research in Boulder and San Diego Supercomputer Center in San Diego. We acknowledge data from NSO Kitt Peak, ESA-NASA SOHO/LASCO project, and the NASA's National Space Science Data Center. We thank Murray Dryer for reviewing the manuscript.

REFERENCES

Linker J. A., and Z. Mikic, *Astrophys. J., 438,* L45-L48, 1995.

Linker J. A., Z. Mikic, R. Lionello, P. Riley, T. Amari, and D. Odstrcil, *Phys. Plasmas, 10,* 1971-1978, 2003.

Mikic, Z., and J. A. Linker, *Astrophys. J., 430,* 898-912, 1994.

Odstrcil, D., M. Dryer, and Z. Smith, *J. Geophys. Res., 101,* 19,973-19,984, 1996.

Odstrcil, D., and V. J. Pizzo, *J. Geophys. Res., 104,* 28,225-28,239, 1999.

Odstrcil, D., J. A. Linker, R. Lionello, Z. Mikic, P. Riley, V. J. Pizzo, and J. G. Luhmann, *J. Geophys. Res., 107,* doi:10.1029/2002JA009334, 2002a.

Odstrcil, D., J. A. Linker, R. Lionello, Z. Mikic, P. Riley, V. J. Pizzo, and J. G. Luhmann, In: *Proc. 10th European Solar Physics Meeting,* ESA SP-506, pp. 95-98, 2002b.

Odstrcil, D., P. Riley, and X. P. Zhao, *J. Geophys. Res., submitted,* 2003.

Riley, P., J. A. Linker, and Z. Mikic, *J. Geophys. Res., 106,* 15,889-15,901, 2001.

Toth, G., and D. Odstrcil, *J. Comput. Phys., 128,* 82-100, 1996.

Webb, D. F., R. P. Lepping, L. F. Burlaga, C. E. DeForest, D. E. Larson, S. F. Martin, S. P. Plunkett, and D. M. Rust, *J. Geophys. Res., 105,* 27,251-27,259, 2000.

Zhao, X. P., S. P. Plunkett, and W. Liu, *J. Geophys. Res., 107,* doi:10,1029/2001JA009143, 2002.

© European Space Agency • Provided by the NASA Astrophysics Data System